Journal of the European Ceramic Society **14** (1994) 481–492

On the Mechanism of Delamination Fracture of $BaTiO_3$-based PTC Thermistors

C. Dewitte,*[a] R. Elst[b] & F. Delannay‡[a]

[a] Université catholique de Louvain, Département des sciences des matériaux et des procédés, PCIM, Place Sainte Barbe 2, B-1348 Louvain-la-Neuve, Belgium
[b] Philips S.A., Avenue Ciceron 1, 1040 Bruxelles, Belgium

(Received 20 December 1993; revised version received 3 June 1994; accepted 6 June 1994)

Abstract

Delamination fracture of positive temperature coefficient PTC thermistors is a mode of thermal shock failure which manifests itself by cracking of the ceramic along a plane approximately parallel to the electrodes. This mode of failure is observed in high-power switching applications. It results from the build-up of thermal stresses whose amplitude is governed by a large number of geometrical, electrical and thermomechanical parameters. An experimental procedure is proposed for the quantitative evaluation of the thermal shock resistance of PTC thermistors. This resistance is characterized by a 'fracture voltage' defined as the voltage causing an increase by more than 10% of the room-temperature resistance after less than 25 switching cycles. The crack trajectory during the successive cycles is revealed by microscopic observation of the fracture surfaces. These experimental results are interpreted by comparison with the temperature and stress distributions computed using a newly developed three dimensional model. This modelling allows evaluation of the relative importance of the parameters affecting failure. The cracking mechanism can be partly elucidated on the basis of the computations of the maps of the normal stresses arising in homogeneous and non-homogeneous ceramics.

Der Bruch durch Ablösung in PTC Thermistoren ist eine durch Thermoschock verursachte Art des Versagens und resultiert in der Rißbildung entlang einer Ebene, die etwa parallel zu den Elektroden verläuft. Diese Art des Versagens wird bei Hochleistungsschaltanwendungen beobachtet. Verursacht wird dies durch thermische Spannungen, wobei die Spannungsamplitude durch eine Vielzahl geometrischer, elektrischer und thermomechanischer Parameter bestimmt wird. Es wird ein experimentelles Verfahren zur quantitativen Bestimmung des PTC-Thermistor-thermoschockwiderstands vorgestellt Der Widerstand wird durch eine 'Bruchspannung' charakterisiert, welche durch die Spannung definiert ist bei der der Raumtemperaturwiderstand nach weniger als 25 Schaltzyklen, um 10% zunimmt. Die Bestimmung des Rißpfads während der folgenden Zyklen erfolgt mittels Mikroskopie der Bruchflächen. Die experimentellen Ergebnisse wurden mit den Temperatur- und Spannungsverteilungen, die sich aus einem neu entwickelten dreidimensionalen Modell ergeben, verglichen. Dieses Modell erlaubt es, die Bedeutung der bruchbeeinflussenden Parameter genauer zu bestimmen. Der Rißmechanismus kann teilweise auf der Grundlage der berechneten Normalspannungen in homogenen und nicht homogenen Keramiken erklärt werden.

La rupture par délamination de thermistances à coefficient de température positif (CTP) est un mode de défaillance par choc thermique qui se manifeste par une fissuration de la céramique suivant un plan approximativement parallèle aux électrodes. Ce mode de défaillance est observé dans les applications de protection de circuits haute puissance. Il découle de la formation de contraintes thermiques dont l'amplitude est gouvernée par un grand nombre de paramètres géométriques, électriques, et thermomécaniques. Une procédure expéri-mentale est proposée en vue de l'évaluation quantitative de la résistance au choc thermique de thermistances CTP. Cette résistance est caractérisée par une 'tension de rupture' définie comme la tension provoquant une augmentation de plus de 10% de la résistance électrique à température ambiante après moins de

* Present address: NGK Ceramics Europe S.A., 1 rue des Azalées. B—7331 Baudour, Belgium.
‡ To whom correspondence should be addressed.

Journal of the European Ceramic Society 0955-2219/94/$7.00 © 1994 Elsevier Science Limited, England. Printed in Great Britain

25 cycles de basculement. La trajectoire de la fissure durant les cycles successsifs est mise en évidence par observation microscopique des surfaces de rupture. Ces résultats expérimentaux sont interprétés par comparaison avec les distributions de température et de contraintes calculées numériquement à l'aide d'un modèle à trois dimensions. Cette modélisation permet de préciser l'importance relative des paramètres affectant la ruine. Le mécanisme de fissuration peut être élucidé en considérant les cartes des contraintes normales dans des céramiques homogènes et non-homogènes.

1 Introduction

Positive temperature coefficient (PTC) thermistors are being used increasingly in applications such as current overload protection (referred to in this paper as 'switching' applications), degaussing devices, or self-regulating heating elements. Their use in high-power switching applications is sometimes limited by the occurrence of mechanical failure by thermal shock as a result of the build-up of thermal gradients in the ceramic. These thermal gradients have two origins: the dissipation toward the external surfaces of the heat generated by the Joule effect and/or the presence of local heterogeneities of properties in the ceramic.

PTC thermistors are usually given the shape of disks with metallic electrodes covering the two base surfaces. Three main modes of mechanical failure have been reported:

(1) the formation of an irregular network of cracks perpendicular to the base surfaces;[1]
(2) the fracture by crack propagation along a plane parallel to the electrodes at approximately mid-distance between them; this mode is called 'delamination fracture';[1–4]
(3) the formation of cracks on the lateral surface of the disk or at the periphery of the electrodes.[2,3,5]

Failure by modes 1 and 3 can, in principle, be prevented by proper processing of the ceramics in such a way as to eliminate heterogeneities and 'hot spots'. Delamination fracture may occur even in the absence of heterogeneities. It is related to the macroscopic thermal gradients whose amplitude is governed by a large number of parameters: geometry of the thermistor, cooling conditions at electrodes and outer surfaces, temperature dependence of the electrical, mechanical and thermal properties of the ceramic.

This paper aims at gaining a better understanding of (i) the mechanism of delamination fracture and (ii) the relative importance of the mentioned parameters on the resistance of the device to this mode of failure. The approach is both experimental and theoretical. An experimental procedure is proposed for the quantitative evaluation of the thermal shock resistance of PTC thermistors in conditions similar to those which prevail in switching applications. The experimental results are interpreted by comparison with the results of three-dimensional numerical computations of the temperature and stress distributions during switching, both in homogeneous thermistors and in thermistors containing local electrical heterogeneities.

Several authors have already attempted to model the temperature distribution arising in a PTC thermistor during switching. Löser Mattheck,[6] Lübitz[1] and Schnabel & Quadflieg[7] used a one-dimensional model based on a macroscopic resistivity function and a convection law. Mader *et al.*[5] used a similar one-dimensional model in which they distinguish the resistivity of the bulk of the grains from that of the grain boundaries. These computations indicate the occurrence of temperature differences of the order of 20 to 40K between the centre and the surfaces of the thermistor. It is found that differences of 10 to 50K may build up between grains of different sizes. These thermal gradients could be monitored by infrared microscopy.[5] From their one-dimensional modelling of the temperature gradients, Schnabel & Quadflieg[7] and Mader *et al.*,[5] computed the stress distributions for a plane-stress field. It was shown that the compressive stresses which arise in the central part of the thermistor during heating become tensile when the Curie temperature is exceeded, as a result of the contraction of the lattice corresponding to the ferroelectric–paraelectric phase transformation. The stresses again become compressive after further heating. Kulwicki[2] reported computations of the temperature and stress distributions based on a three-dimensional model making use of a combination of finite differences and finite elements methods. It was suggested that the delamination surface corresponds to the locus of the maximum tensile stresses.

In the present paper, the approach followed in these former works is extended by the introduction of a fully tridimensional numerical model taking into account the heat dissipation both at the electrodes and at the lateral surfaces of the thermistor.[8] Comparison of the computed stress distributions with the morphology of the fracture surfaces throws light on the mechanism of crack propagation during delamination. The computations also allow the influence of the various parameters (geometrical, electrical, mechanical, thermal) controlling the occurence of failure to be evaluated.

2 Methods

2.1 Experimental methods

2.1.1 Materials

The thermistors were disk-shaped commercial-type Sb-doped $Ba_{1-x-y-z}Ca_xSr_yPb_zTiO_3$ ceramics with $x = 0{\cdot}10$, $0 \leq y\ 0{\cdot}07$, and $0{\cdot}06 \leq z \leq 0{\cdot}13$. They were prepared by the conventional mixed oxides method with double layer NiCr + Ag electrodes. Except when stated otherwise in the following, the disks had a radius $R_0 = 5$ mm and a height $d = 3$ mm. Testing of thermal shock resistance was carried out on a large variety of batches of samples. In order to limit the number of parameters affecting failure, all batches chosen for this investigation exhibited approximately the same value of resistance at room temperature $R_{25} \approx 10$–15Ω and the same Curie temperature $T_C \approx 120°C$. The other electrical properties varied depending on the composition and processing conditions of the batches.

The electrical properties of each of the batches were characterized by measuring the dependence of resistance versus temperature (R/T curve) and the dependence of current versus voltage (I/V curve). From the R/T curve, the main electrical properties of a PTC thermistor are derived: Curie temperature T_C (°C); resistivity at room temperature ρ_{25} (Ω cm); slope of the PTC effect μ_2 (%K^{-1}) (μ_2 is the slope of the raising part of the R/T curve on a semi-logarithmic plot: see relation (3) later). From the I/V curve, one determines the voltage V_{max} corresponding to the thermal runaway of the thermistor, i.e. to the onset of the negaive temperature coefficient (NTC) part on the R/T curve.

The density of the ceramics was measured by the Archimedean method. Optical microscopy and SEM were used for measuring the grain sizes, for monitoring the presence of secondary phases and for characterizing the crack extension mode on the fracture surfaces. Actually, the differences in microstructure between the batches studied in this work were fairly limited: the relative densities amounted to $88{\cdot}8 \pm 2{\cdot}5\%$ and the grain sizes (de Heyn sizes) averaged $4{\cdot}6 \pm 0{\cdot}5$ μm. The differences of composition were also very small as they concerned only minor additions. Hence, when discussing the results, it will be assumed that the effect of possible differences of mechanical properties can be neglected in comparison to the effect of the differences of electrical properties.

2.1.2 Testing of thermal shock fatigue resistance

Figure 1 sketches the experimental setup that was developed for testing the shock resistance under 'switching' conditions. The sample cell consists of two copper electrodes in good thermal contact with water-cooled heat sinks. The thermistor is inserted between these electrodes using a conducting paste made of Ag powder and silicone. The setup includes an AC (50 Hz) power supply (maximum 250 V, 30 A), a low ohmic resistor R_v ($\approx 10^{-2}\ R_{25}$) in series with the thermistor, an ohmmeter, a storage oscilloscope and a computer for piloting the test.

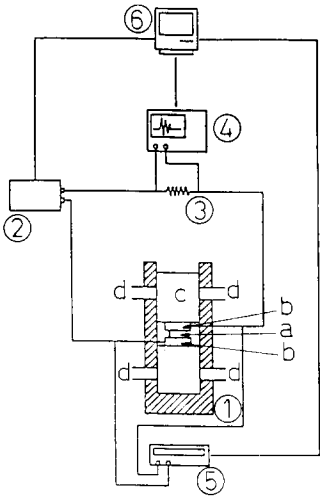

Fig. 1. Experimental set-up for thermal shock resistance tests. (1) Specimen cell; (a) thermistor; (b) copper electrodes; (c) water-cooled sinks; (d) water supplies; (2) power supply; (3) series resistor; (4) oscilloscope; (5) ohmmeter; (6) computer.

The 'thermal shock fatigue resistance' is tested by exposing the sample to a succession of cycles consisting in:

—applying a given AC voltage V for 5 s while recording the transient current;
—allowing the sample to cool down to 25°C (room temperature): about 45 s were usually sufficient;
—measuring R_{25}.

This cycle was repeated using the same value of V until an increase of R_{25} was recorded, which indicated that damage (cracking) had developed within the sample. The test was then either stopped in order to characterize this damage or continued until fracture by delamination was completed. If no change of R_{25} was detected after 25 cycles, a new series of cycles with a higher voltage V was started. The whole sequence of cycles was controlled by computer. (The values of V mentioned in the following are the effective values of the AC voltage.)

The magnitude of the inrush current at the onset of the voltage (i.e. the magnitude of the thermal shock) may be reduced by increasing the value of the resistor R_v in series with the thermistor. However, unless stated otherwise, all (experimental and modelling) results presented in the following were obtained under the most drastic shock conditions, i.e. with $R_v = 0{\cdot}15\ \Omega$.

2.2 Modelling methods

The modelling is based on the hypotheses of the theory of linear, uncoupled and quasi-static thermoelasticity. This means that one neglects the mechanical coupling terms in the energy equations (i.e. temperature is assumed not to depend on deformation) and that one omits the inertia terms in the motion equations. These hypotheses are valid in the present case because of (i) the relatively low value of the maximum temperature in the ceramic during switching (150°C to 250°C, as it will be shown later) and (ii) the absence of plasticity of the ceramic.

In such conditions, the mathematical equations can be separated into two sets which may be solved consecutively. First, the evolution of the temperature distributions in the ceramic is computed from the equations for heat conduction with a source term corresponding to the local generation of heat by the Joule effect. Thereafter, these temperature distributions are used, together with the proper boundary conditions, for computing the thermal stresses from the 15 equations of thermoelasticity (3 equilibrium conditions, 6 stress–strain relations and 6 strain–displacement relations). (When stresses and strains are due to temperature alone, the effects of density and volume forces can be neglected.)

These two sets of equations and the numerical methods used for solving them are presented in the Appendix.[8,9] Owing to the geometry of the thermistors, use is made of cylindrical coordinates with rotational symmetry.

It was assumed that the thermal conductivity k, the density δ, the Young's modulus E, and the Poisson coefficient ν were independent of temperature: $k = 0{\cdot}025$ W cm^{-3}, $\delta = 5{\cdot}6$ g cm^{-3}, $E = 100$ GPa, and $\nu = 0{\cdot}33$. (According to Mader *et al.*,[10] the Young's modulus is about 20% higher above T_C than below T_C. However, this variation was considered small enough to be neglected at the present stage of the modelling.)

The temperature dependence of the other physical properties of the ceramic was expressed using a non-dimensional temperature θ defined as

$$\theta = \frac{T - T_C}{T_C} \tag{1}$$

where T_C is the Curie temperature (fixed at 120°C in the present work). The temperature dependences of the heat capacity $C(\theta)$, resistivity $\rho(\theta)$, and thermal expansion $s(\theta) = \alpha(T - T_0)$ were then expressed using the relations proposed by Schnabel & Quadflieg:[7]

$$C(\theta) = C_0[1 + C_1\theta + C_2 \exp(\pm\lambda\theta)] \tag{2}$$

with $C_0 = 523$ W skg^{-1} K^{-1}, $C_1 = 0{\cdot}024$, $C_2 = 0{\cdot}296$, $\lambda = 3$ and the sign + or − when θ is negative or positive, respectively.

$$\rho(\theta) = \rho_0 \exp(\mu_i\theta) \tag{3}$$

where $\mu_i = -\mu_1$ for $\theta \leq 0$ and $\mu_i = \mu_2$ for $\theta > 0$. The three parameters μ_1, μ_2 and ρ_0 are defined by drawing, on a semilogarithmic ρ/T diagram, the two straight lines which best fit the dependence of the resistivity of the PTC thermistor as a function of the temperature. μ_2 is the slope of the PTC effect.

$$s(\theta) = \alpha(T - T_0) = \alpha T_0(\theta - \theta_0)$$

$$s(\theta) = T_0\left[\alpha_1(\theta - \theta_0) - \frac{\beta_1}{\sigma_1}\exp(\sigma_1\theta)\right] \text{ for } \theta \leq 0 \tag{4}$$

and

$$s(\theta) = T_0\left\{\alpha_2\theta - \alpha_1\theta - \frac{\beta_1}{\sigma_1} - \frac{\beta_2}{\sigma_2}\right.$$
$$\left.[1 - \exp(-\sigma_2\theta)]\right\} \text{ for } \theta > 0 \tag{5}$$

with $T_0 = 25$°C, $\alpha_1 = 7{\cdot}8 \times 10^{-6}$ K^{-1}, $\alpha_2 = 12{\cdot}0 \times 10^{-6}$ K^{-1}, $\beta_1 = 14{\cdot}8 \times 10^{-6}$ K^{-1}, $\beta_2 = 19{\cdot}0 \times 10^{-6}$ K^{-1}, $\sigma_1 = 1{\cdot}65$ and $\sigma_2 = 2{\cdot}00$. These expressions account for the effect of the contraction of the lattice during the phase transformation, which brings about an apparent negative expansion coefficient in a certain temperature interval above T_C.

The effect of a local heterogeneity of electrical properties on the temperature and stress distributions was computed by modifying the value of ρ_0 in relation (3). In order to avoid discontinuities which would impair the convergence of the numerical computations, it was assumed that ρ_0 varies along the whole z and r range according to a Gaussian law. The maximum of ρ_0 was chosen equal to 10 times or 100 times its value far from the heterogeneity. This maximum was located on the median plane of the disk, either at the centre or on the lateral surface.

Whereas the experiments were carried out using an AC power supply, the voltage V used in the modelling was considered constant for $t > 0$.

3 Experimental Results

3.1 Thermal shock fatigue resistance

Figure 2 presents the variation of R_{25} as a function of the number of cycles for three samples of the same batch submitted to voltages of 110, 120 and 130 V. Three different behaviours are observed.

—When $V = 110$ V, no change of R_{25} is recorded: the thermistor is left undamaged.
—When $V = 120$ V, the curve exhibits a gradual increase of R_{25}: the thermistor is damaged but not completely broken.

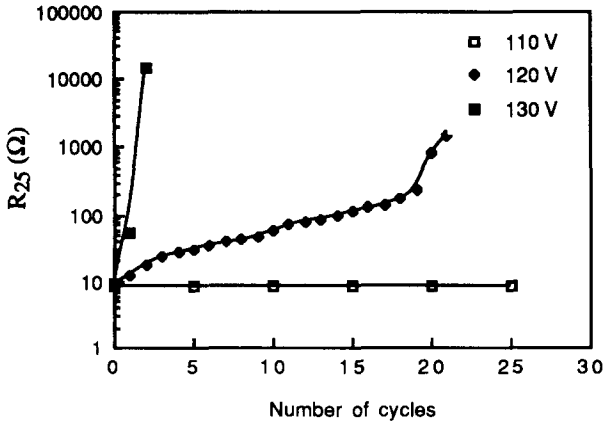

Fig. 2. Variation of R_{25} as a function of the number of cycles for three specimens of the same batch exposed to different applied voltages V.

—When V = 130 V, R_{25} increases abruptly and the thermistor has completely broken by delamination after 3 cycles.

Designating R_{25n} the value of R_{25} after n cycles, another way to present the same results is to plot, as shown for example in Fig. 3, the variation of $(1 - R_{25o}/R_{25n})$ as a function of the voltage V for a given number of cycles n. Usually, the transition to the upper plateau ($R_{25n} \rightarrow \infty$) occurred in a very narrow voltage interval.

Finally, it is also useful to present the results in a similar way as for the so-called Wöhler curves in mechanical fatigue. For this purpose, as failure criterion, the observation of an increase of R_{25n}/R_{25o} by more than 10% is used. Figure 4 shows an example of the variation of the voltage corresponding to this failure criterion as a function of the number of cycles. Each point is an average over 5 samples of the same batch. This procedure enables the shock resistance of a batch of samples to be characterised by its 'failure voltage', V_{fract}, that is defined as the minimum voltage V for which an increase of R_{25} by more than 10% is observed before the completion of 25 cycles. For example, in the case of the batch of Fig. 4, V_{fract} = 120 V.

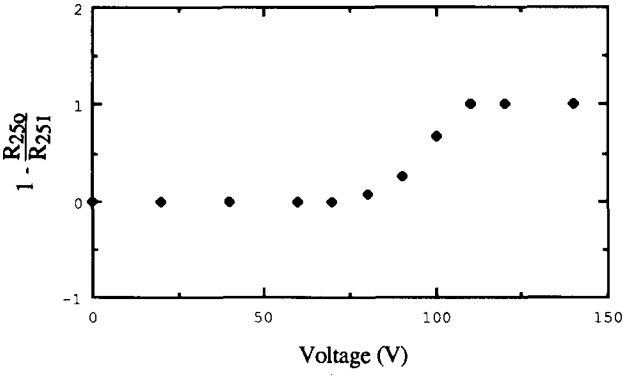

Fig. 3. Example of the relative change of R_{25} after 1 cycle as a function of the applied voltage V for specimens belonging to the same batch.

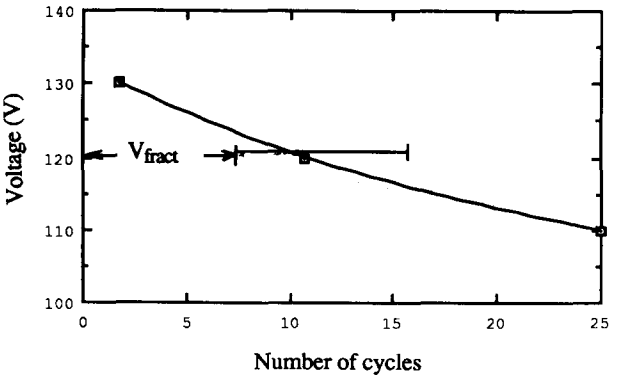

Fig. 4. Example of a 'thermal shock fatigue curve' for a particular batch of samples. The minimum voltage V causing a 10% increase of R_{25} after n cycles is plotted as a function of the number of cycles.

The failure voltage V_{fract} of the different batches which were investigated varied from 50 V up to more than 240 V. (Actually, due to the limitations of the power supply, it was not possible to measure the failure voltage of the batches with V_{fract} > 240 V.) Although the value of V_{fract} was dependent on the whole R/T curve of the ceramics, the most important parameter appeared to be the value of the PTC slope μ_2. Figure 5 summarizes the variation of V_{fract} as a function of the PTC slope for different batches. Batches with low values of V_{fract} (50 to 70 V), medium values of V_{fract} (90 to 120 V), and very high values of V_{fract} (>240 V) exhibit PTC slopes of 5–8% K^{-1}, 8–12% K^{-1}, and around 20% K^{-1}, respectively.

3.2 Fractography

The aspect of the fracture surfaces could be correlated to the evolution of R_{25} measured at the end of the successive fatigue cycles. Figures 6 and 7 show micrographs of typical fracture surfaces of thermistors which had broken by delamination

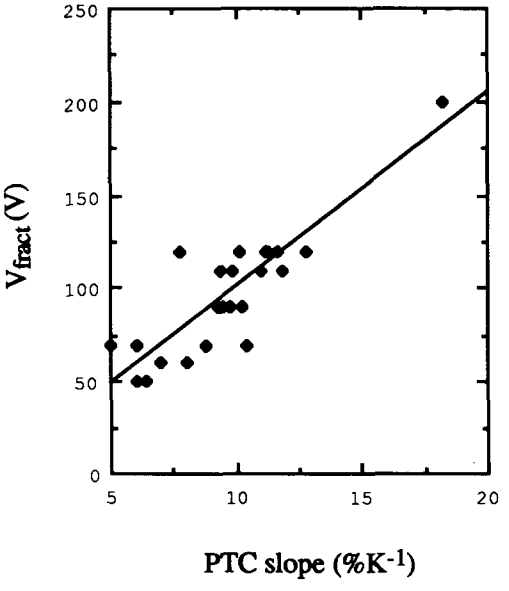

Fig. 5. Variation of V_{fract} as a function of the PTC slope for a set of different batches of thermistors.

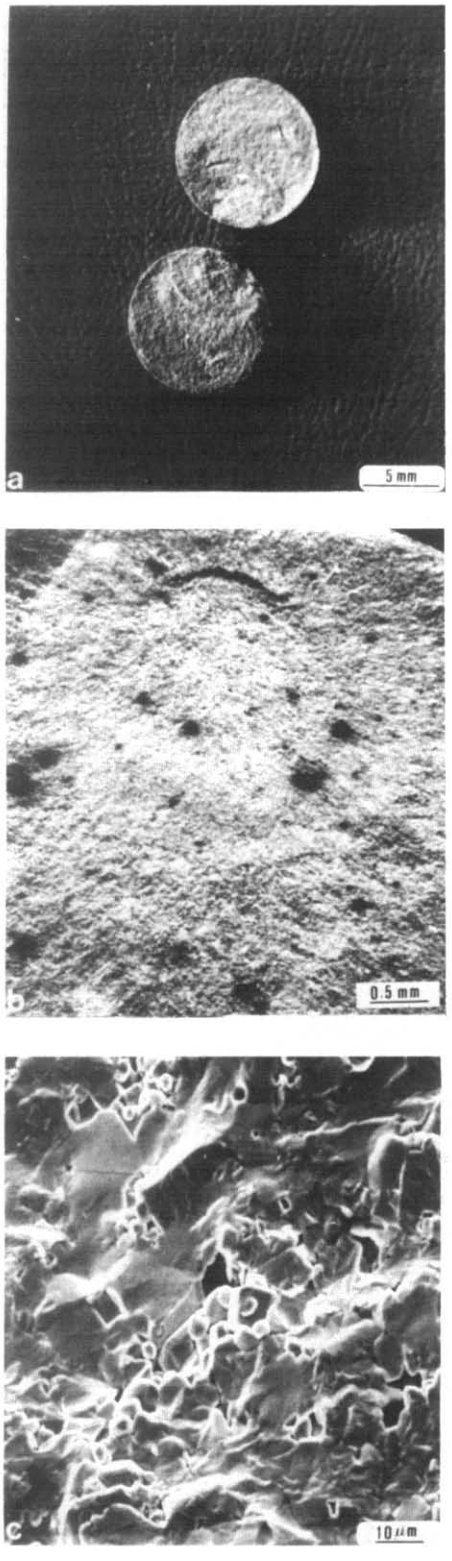

Fig. 6. Fracture surface of a thermistor having broken by delamination after only a couple of cycles. (a) General view of the two parts. (b) Detail of the area in the centre of the ridges. (c) SEM micrograph showing transgranular cracking.

after 1–3 cycles or after 10–20 cycles, respectively. The fracture surfaces present a set of concentric ridges whose number was found to correspond to the number of cycles before completion of the fracture. The fracture mode between these ridges is clearly transgranular. It seems that the ridges localize the position of crack arrests during the successive cycles.

In the case of the samples having broken after more than 10 cycles (Fig. 7), one observes in addition a ring presenting a different facies at the periphery of the fracture surface. Figure 7(d) suggests that the fracture mode within this ring is intergranular.

These observations did not allow the author to determine for sure whether the crack had extended from the lateral surfaces toward the centre of the disks or had nucleated at a heterogeneity in the bulk and extended thereafter toward the lateral surfaces. However, as shown in Fig. 8(a), a crack could often be observed on the lateral surface at mid-distance from the electrodes in the case of thermistors which had exhibited a slow increase of R_{25} during a few successive cycles but were still unbroken. As shown in Fig. 8(b) a transverse section of such a damaged thermistor revealed the extension of a crack from the lateral surface.

In order to gain a better insight into the role of possible cracks nucleating on lateral surface, a set of thermistors having a notch (250–800 μm depth $\times$ 500 μm width) machined on this surface along the whole periphery using a diamond saw was also tested. In comparison to the unnotched thermistors, R_{25} after the first cycle increased by about 50%, V_{fract} decreased by about 50%, and the increase of R_{25} during the successive cycles was much slower. As shown in Fig. 9, a transverse section of such a notched specimen exposed to a few switching cycles exhibited the presence of a crack having extended from the notch.

4 Modelling Results and Discussion

4.1 Temperature distributions

Figure 10 presents, for a homogeneous thermistor, the graphs of the temperature distributions along r in the median plane ($z = d/2$) and along z on the axis of the disk ($r = 0$) for different times after the application of a voltage step $V = 170$ V. The specific parameters used in the computation are given in the legend of the figure. It is useful to extract from these graphs the evolution of the temperatures and temperature gradients at some characteristic locations in the thermistor. For example, Fig. 11 shows, for the same parameters of computation, the evolution of the temperature in the median plane, at the centre ($z = d/2$, $r = 0$) and on the lateral surface ($z = d/2$, $r = R_0$). The temperature reaches T_C after 0·3 s and stabilizes at about T_C + 25°C for $t > 1$ s. This later temperature will be called in the following the equilibrium temperature T_{eq}.

The thermal stresses being driven by the temperature gradients, it is also instructive to draw, as

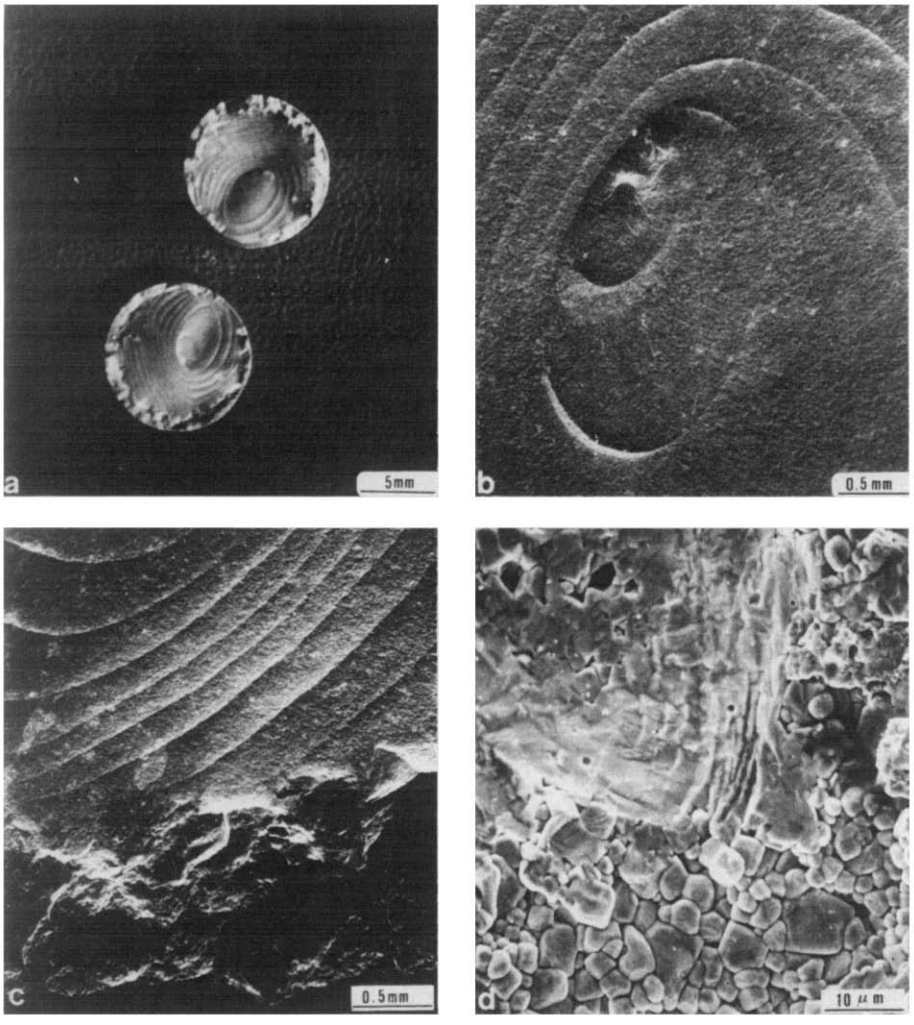

Fig. 7. Fracture surface of a thermistor having broken by delamination after more than 10 cycles. (a) General view of the two parts. (b) Area around the centre of the concentric ridges. (c) Area close to the border between the external ring and the ridges. (d) SEM micrograph showing a transition from intergranular fracture in the external ring to transgranular fracture in the ridged area.

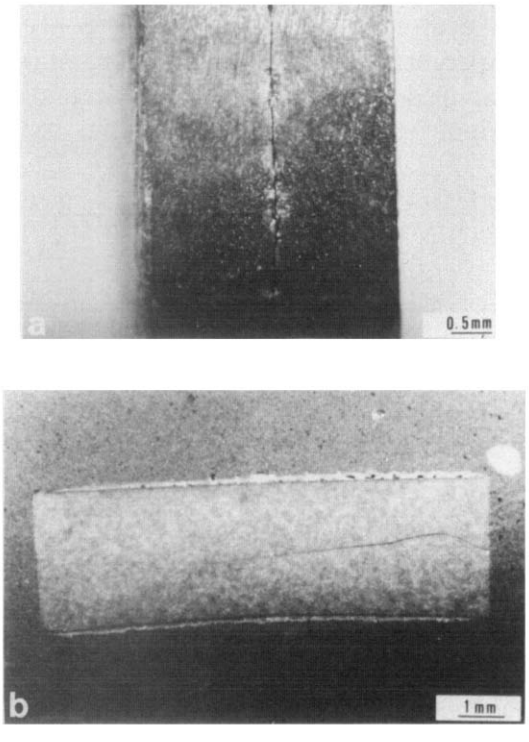

Fig. 8. (a) Crack observed on the lateral surface at mid-distance from the electrodes in the case of a thermistor having exhibited a slow increase of R_{25} during a few successive cycles. (b) Transverse section of such a thermistor revealing the extension of a crack from the lateral surface.

shown in Fig. 12, the distributions of the temperature gradients dT/dz along the axis and dT/dr along the distance r from the axis in the median plane. All gradients increase from the external surfaces toward the centre of the disk. The radial gradient dT/dr is significant only within a narrow ring along the lateral surfaces.

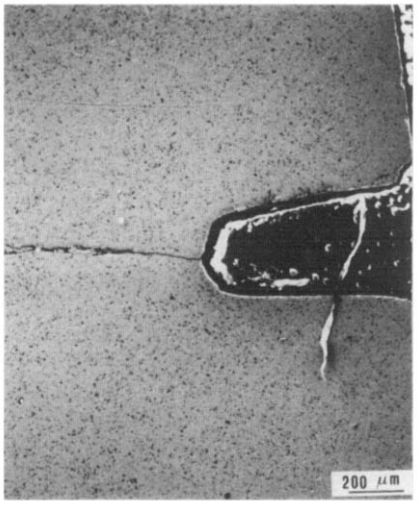

Fig. 9. Transverse section of a notched specimen exposed to a few switching cycles, exhibiting the presence of a crack having extended from the notch.

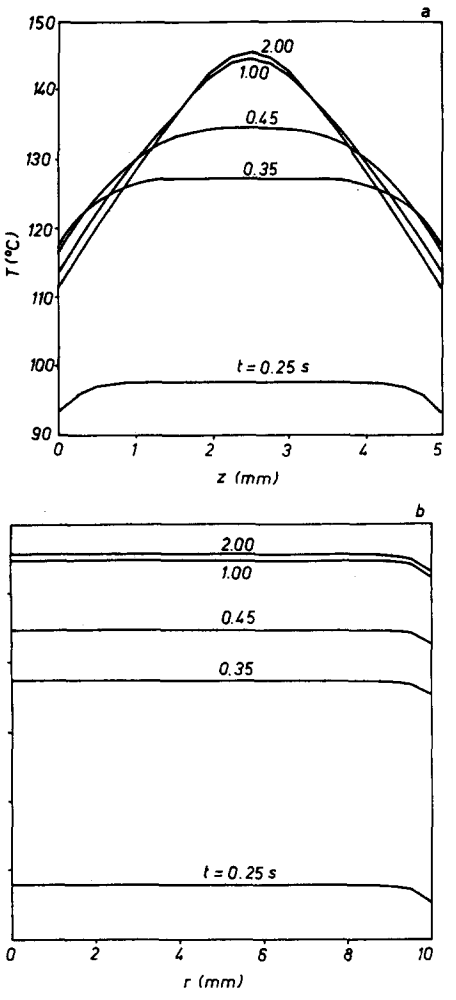

Fig. 10. Temperature distributions in a homogeneous thermistor (a) along r in the median plane ($z = d/2$) and (b) along z on the axis of the disk ($r = 0$) for different times (in seconds) after the application of a voltage step $V = 170$ V. The parameters used in the computations are $T_0 = 20°C$, $d = 5$ mm, $R_0 = 10$ mm, $\rho_0 = 100$ Ωcm, $\mu_1 = 0{\cdot}1$, $\mu_2 = 4{\cdot}5$, $h_r = 250$ WK^{-1} m^{-2}, $h_z = 500$ WK^{-1} m^{-2}. (The significance of the symbols is given in the text or in the Appendix.)

An extensive study has been carried out of the influence of the various parameters of the computation on the magnitude, distribution and rate of increase of the temperatures in the ceramics.[8] Table 1 summarizes qualitatively the results of this study. As a general rule, the gradients increase when the equilibrium temperature T_{eq} increases.

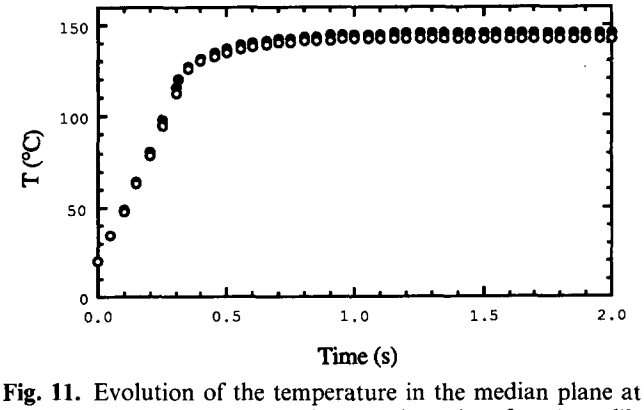

Fig. 11. Evolution of the temperature in the median plane at the centre ($z = d/2$, $r = 0$) and on the lateral surface ($z = d/2$, $r = R_0$). (Same parameters of computation as in Fig. 10.)

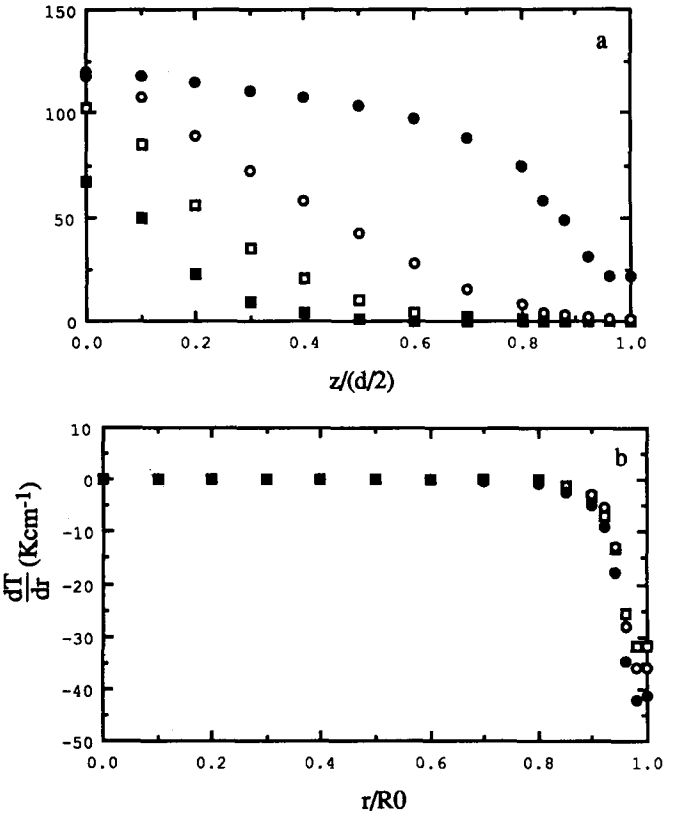

Fig. 12. Distributions of the temperature gradients: (a) dT/dz along the axis; (b) dT/dr along the distance r from the axis in the median plane. (Same parameters of computation as in Fig. 10.) ■, $t = 0{\cdot}25$ s; □, $t = 0{\cdot}35$ s; ○, $t = 0{\cdot}45$ s; ●, $t = 2$ s.

The four last lines of Table 1 concern parameters which are fixed by the experimental conditions of the thermal shock fatigue test. T_C being constant at about 120°C for all the batches studied in this work, the three first lines of Table 1 concern the main experimental variables. Obviously, an increase of the applied voltage V causes an increase of the equilibrium temperature T_{eq} and of the maximum heating rate $(d\theta/dt)_{max}$, i.e. an increase of the amplitude of the thermal shock. It may be noticed also that the effect of an increase of the applied

Table 1. Qualitative influence of the computation parameters on the temperatures

Parameter	T_{eq}	$\Delta T_{z\ axis}$	$\Delta T_{r\ median}$	$(d\theta/dt)_{max}$
V	+	(+)	(+)	+
μ_2	−	−	−	=
ρ_0	−	(−)	(−)	−
T_C	+	+	=	=
k	−	−	−	=
R_0	=	=	+	=
d	(−)	+	+	−
h_z	=	+	=	−
h_r	=	=	+	=

T_{eq}: equilibrium temperature, $\Delta T_{z\ axis}$: temperature differences between the centre and the surface along the axis; $\Delta T_{r\ median}$: idem along the radius in the median plane; $(d\theta/dt)_{max}$: maximum heating rate at the centre; +, −, or = indicate an increase, a decrease, or no significant change, respectively, when the parameter increases. Parentheses mean that the change is weak.

Table 2. Computation of the equilibrium temperature T_{eq} and temperature differences $\Delta T_{z\ axis}$ and $\Delta T_{r\ median}$ (see definitions in Table 1) using the experimental parameters measured for 5 batches of thermistors

Code	*Experimental parameters*					*Results of computations*		
	d *(mm)*	R_0 *(mm)*	μ_2 *(% K^{-1})*	ρ_0 *(Ω cm)*	V_{fract} *(V)*	T_{eq} *(°C)*	$\Delta T_{z\ axis}$ *(°C)*	$\Delta T_{r\ median}$ *(°C)*
23201	3	5	10·1	16·1	120	184	27	0·5
2-A-10	3	5	12·8	16·7	120	173	25	0·5
2-A-05	3	5	8·0	14·3	60	180	27	0·5
2-F-10	3	5	11·3	14·8	60	179	26	0·5
18	2·6	8	18·2	55·3	200	176	22	0·5

voltage V can be compensated by an increase of the PTC slope μ_2. This justifies qualitatively the correlation between V_{fract} and μ_2 shown in Fig. 5.

A more precise interpretation of the experimental results requires that the combination of all experimental parameters be taken into account. This exercise has been carried out for only 5 of the 31 batches that have been tested. The results are presented in Table 2. The applied voltage V used in the computations is the value of V_{fract} measured for the batches. It is conspicuous that the computed equilibrium temperature for $V = V_{fract}$ is very closely the same for all the batches considered in Table 2 in spite of the fairly large differences of electrical properties and geometry. This suggests that the intrinsic thermal shock resistance of PTC ceramics may be characterized by the maximum value of T_{eq} that the ceramic can sustain without being damaged.

4.2 Stress distributions

It can be assumed that, as observed usually in isotropic materials, cracks extend in PTC ceramics under mode I, i.e. with $K_{II} = 0$. In this case, the trajectory of a delamination crack can be discussed by considering only the normal stresses σ_{zz} and σ_{rr}. Figure 13 presents, for a homogeneous thermistor, the maps of σ_{zz} and σ_{rr} on a transverse section,

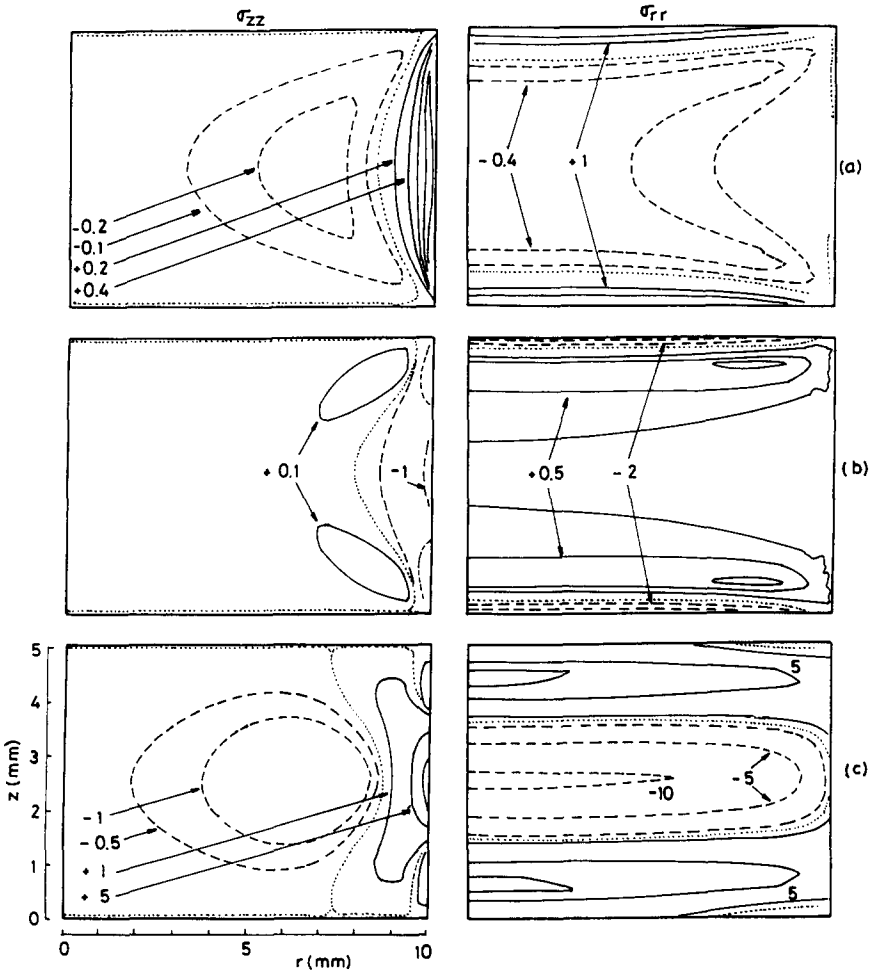

Fig. 13. Maps of σ_{zz} and σ_{rr} on a transverse section of a homogeneous thermistor at (a) t = 0·5 s; (b) t = 0·8 s; (c) t = 1·7 s. The loci of tension stresses are represented by full lines, those of compression stresses by dashed lines and the locus of zero stress by a dotted line. The parameters of the computation are the same as for Fig. 10. The stress units are MPa.

computed for three different times after the onset of the voltage. The magnitudes of σ_{zz} and σ_{rr} are related to the temperature gradients in the r and z directions, respectively. Their sign depends on the sign of the apparent thermal expansion coefficient. The centre of the thermistor being hotter than the surfaces, one observes compressive stresses in the centre and tensile stresses in the vicinity of the surfaces both at the beginning (t = 0·5 s) and the end (t = 1·7 s) of the heating cycle. The reverse is observed for t = 0·8 s. This anomaly is due to the fact that, at this time, the temperature of the centre is within the temperature interval close to T_C where the contraction of the lattice due to the ferroelectric–paraelectric phase transformation causes an apparent negative thermal expansion.

The maps of Fig. 13 suggest that, in homogeneous thermistors, a delamination crack is most likely to originate from the lateral surface at mid-distance from the electrodes where the stresses σ_{zz} are the most tensile. Such a crack would arrest when entering the compressive zone ahead of it. As seen in Fig. 13(c), near the transition between the tensile and compressive zones, both normal stresses σ_{zz} and σ_{rr} increase toward the electrodes. Hence, the crack may be driven away from the median plane before arresting. Such phenomena of crack deflection and arrest during each cycle would justify the formation of the concentric ridges observed on the delamination surface in Fig. 7.

However, two objections may be raised about this discussion of the cracking mechanism on the mere basis of stress maps in a continuum body: (1) the intensities of the computed stresses are low and (2) the influence of the presence of a crack has not been taken into account. These points will be dealt with successively in the following sections.

4.3 Stress intensities and influence of heterogeneities

The magnitude of the normal stresses in the maps of Fig. 13 is quite low. The maximum of the computed σ_{zz} at the surface (which is obtained when the equilibrium temperature distribution is reached) amounts to about 15 MPa (Fig. 13(c)). This value is much lower than the fracture strength of PTC ceramics which is of the order of 100 MPa.[11–14] It was shown by Dewitte[8] that the magnitude of the stresses is significantly affected by the value of the parameters chosen for the computation. However, it is slightly plausible that normal stresses of the order 100 MPa be reached locally in a homogeneous thermistor. Nevertheless, it may be advocated that the intergranular cracking mode observed at the periphery of the disk in Fig. 7 may correspond to a subcritical crack extension which could have been driven by much lower stresses than the fracture strength. Fast transgranular cracking could initiate later when the subcritical crack reaches a critical size (Fig. 8).

In order to gain some insight into the role of local heterogeneities of electrical properties, computations have been performed with local variations of ρ_0 introduced in the model. In order to allow numerical convergence, the spatial distributions were given by a Gaussian profile. Several different cases have been considered.[8] As an example, Fig. 14 presents the evolution of σ_{zz} in the median plane ($z = d/2$) at the centre (r = 0) and on the lateral surface ($r = R_0$) when a heterogeneity with ρ_0 max = 10 $\rho_{0\ \text{nominal}}$ is located either on the lateral surface (Fig. 14(a)) or on the axis (Fig. 14(b)). Figure 14(a) presents also the evolution of the maximum of σ_{zz} in the median plane. In comparison to the homogeneous case, the magnitude of the stresses is, in both cases, much larger and significant tensile stresses (≈40 MPa) are present in the bulk of the thermistor.

These results indicate that local heterogeneities may bring about stress concentrations which may be high enough to induce the nucleation of a crack in the bulk of the ceramic. During the subsequent switching cycles, this crack could extend progressively toward the lateral surface by forming concentric ridges. Such a mechanism is a possible

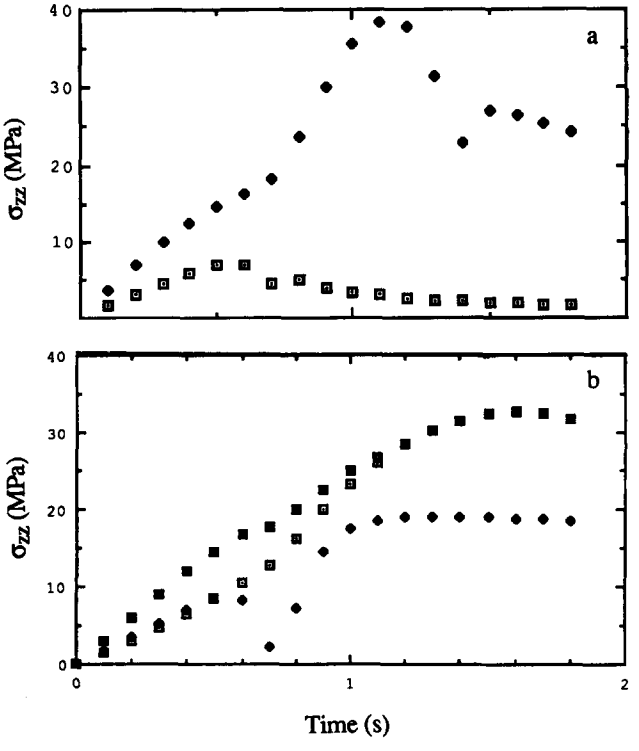

Fig. 14. Evolution of σ_{zz} in the median plane ($z = d/2$) at the centre (r = 0) and on the lateral surface ($r = R_0$) in the presence of an heterogeneity with $\rho_{0\ \text{max}} = 10\ \rho_{0\ \text{nominal}}$. (a) Heterogeneity located on the lateral surface; (b) heterogeneity located on the axis. $\sigma_{zz\ \text{max}}$ is the maximum of σ_{zz} in the median plane. The parameters of the computation are the same as for Fig. 10. □, σ_{zz} (r = 0, $z = d/2$); ◆, σ_{zz} ($r = R_0$, $z = d/2$)s; ■, $\sigma_{zz\ \text{max}}$ (r, $z = d/2$).

alternative to the mechanism of crack extension from the lateral surface, which has been suggested on the basis of the stress maps in homogeneous ceramics.

A notch can be considered as an extreme case of an heterogeneity with a higher resistivity than the bulk of the ceramics. It will thus also induce an enhancement of the stresses. This enhancement may explain the lower value of V_{fract} which was measured for notched ceramics and the crack extension observed after a few cycles at the tip of the notch in Fig. 9.

4.4 Fracture mechanics considerations

A major limitation of this discussion of the cracking mechanism on the basis of stress maps and stress intensities is the hiding of the fact that the formation of a crack modifies very significantly the stress field. A more precise insight into the phenomenon would require the computation of the time dependence of the strain energy release rate G of an incipient crack along the median plane in the thermistor. The computation of the variation of G as a function of crack length and crack orientation should allow one to justify the phenomena of crack deflection and arrest. Such a modelling combining electricity, thermoelasticity, and fracture mechanics necessitates a more elaborate computation model which has not yet been developed.

Much interest has arisen in the recent literature about the understanding of cracking in ferroelectric ceramic multilayers used as large strain actuators.[15–18] In contrast to PTC thermistors, the ferroelectric ceramics in such devices are supposed to remain perfect insulators. Hence, it is believed that cracking is then not driven by thermal stresses but by electrostrictive strains caused by the electric field. It might be argued that a similar situation prevails in a PTC when the ceramic has become insulating after switching. It has been shown by several authors[15,16] that, for a crack perpendicular to the electric field, the driving force deriving from electrostriction is negative when the crack is more insulating than the ceramic. This situation is certainly applicable for a crack in a PTC. However, Cao *et al.*[18] have proposed that, at patches of contact of the crack faces, the distorsion of the electric field may cause a local expansion, leading to a wedging action on the crack. More work is obviously needed before an assessment can be made of the possibility of occurence of such a mechanism in PTCs.

5 Conclusions

The conclusions of this work can be summarized as follows.

(1) The thermal shock resistance of a thermistor may be best characterized by the minimum voltage causing a certain amount of damage after a given number of switching operations.

(2) The relative importance of the geometrical, electrical and thermomechanical parameters which determine delamination resistance has been assessed by a three dimensional modelling of the temperature distributions. It appears that failure occurs when a certain value of the equilibrium temperature is exceeded.

(3) The aspect of the fracture surface suggests a mechanism of crack extension and arrest during each switching operation. This mechanism may be partly justified by considering the computed maps of the normal stresses in the ceramics.

(4) The presence of electrical heterogeneities causes a large increase of the thermal stresses. This may allow crack nucleation in the bulk of a thermistor. A more elaborated model including fracture mechanics concepts should be developed in order to describe more properly the role of cracks and the conditions of their extension.

Acknowledgements

The authors acknowledge the collaboration of Prof. J. P. Michenaud and Dr J. Boxus. They are indebted to Dr P. Schnabel for providing unpublished data on the modelling of PTC thermistors. This work was partly supported by IRSIA/IWONL, Belgium and by the Services de Programmation de la Politique Scientifique (Belgium) under contract PAI4.

References

1. Lubitz, K., Switching behaviour of power PTC resistors. *Ber. Deutsch. Keram. Ges.*, **55** (1978) 322–4.
2. Kulwicki, B. M., Instabilities in PTC resistors. In *Proceedings of the 6th International Symposium on the Applications of Ferroelectrics*, IEEE, Bethlehem, PA, 1986, pp. 656–64.
3. Ford, R. & Kahn, M., Positive temperature coefficient resistors as high power pulse switches. In *Proceedings of the 6th International Symposium on the Applications of Ferroelectrics*, IEEE, Bethlehem, PA, 1986, pp. 669–72.
4. Dewitte, C., Keustermans, J. P., Delannay, F., Elst, R. & Michenaud, J. P., Experimental study of the thermomechanical behaviour of barium titanate based PTC thermistors, *Silicates Industriels*, **1990/1–2** (1990) 5–12.
5. Mader, G., Meixner, H. & Kleinschmidt, P., Hot spots in semiconducting ferroelectric ceramics. *Siemens Forsch.-u.-Entwickl. Ber. Bd.*, **14** (1985) 133–9.
6. Löser, W. & Mattheck, C., Theory of thermal switching behaviour of a PTC-resistor device. *Phys. Stat. Sol. (a)*, **18** (1973) 247–54.

7. Schnabel, P. & Quadflieg, P., Internal report, Philips N.V. Aachen, Germany, 1985.
8. Dewitte, C., Etude du comportement thermomécanique de thermistances CTP à base de titanate de baryum, PhD thesis, Université Catholique de Louvain, Belgium, 1990.
9. Dewitte, C., Michenaud, J. P. & Delannay, F. Study of the macroscopic thermal stresses in $BaTiO_3$ based thermistors. In *Proceedings of ECerS '89*, ed. G. de With, R. A. Terpstra & R. Metselaar. Elsevier, London, 1989, pp. 3.232–3.236.
10. Mader, G., Meixner, H. & Kleinschmidt, P., Temperature and stress dependence of Young's modulus in semiconductors barium titanate ceramics. *J. Appl. Phys.*, **58** (1985) 702–4.
11. Pohanka, R. C., Rice, R. W. & Walker, B. E., Effect of internal stress on the strength of $BaTiO_3$. *J. Am. Ceram. Soc.*, **59** (1976) 71–4.
12. de With, G. & Parren, H., Fracture of PTC ceramics. *Sci. Ceram.*, **12** (1984) 537–42.
13. de With, G. & Parren, H., Surface stresses in modified $BaTiO_3$ ceramics. *Proc. Brit. Ceram. Soc.*, **34** (1984) 99–108.
14. de With, G. & Parren, H., Fracture of modified $BaTiO_3$ ceramics. *Silicates Industriels*, **9** (1984) 179–83.
15. McMeeking, M. R., Electrostrictive stress near crack-like flaws. *J. Appl. Math. Phys.*, **40** (1989) 615.
16. Suo, Z., Models for breakdown-resistant dielectric and ferroelectric ceramics. *J. Mech. Phys. Solids*, **41** (1993) 1155.
17. Lynch, C. S., Chen, L., Yang, W., Suo, Z. & McMeeking, R. M., Crack growth in ferroelectric ceramics driven by cyclic polarization switching. In *Proceedings of Adaptative Structures and Materials Systems Symposium*, 1993, in press.
18. Cao, H. C., He, M.-Y. & Evans, A. G., Electric field-induced fatigue crack extension in ferroelectric ceramics. (1993) submitted for publication.
19. Dupret, F., Nicodème, P. & Vanden Bogaert, N., Elastic: Software FEMAG, Université catholique de Louvain, Unité de mécanique appliquée, Louvain-la-Neuve, Belgium, 1986.

Appendix 1: Numerical Methods

Temperature distributions in the presence of an internal heat source Q can be computed from the differential equation

$$k(T)\,\nabla^2 T + Q(T) = \delta(T)C(T)\frac{\partial T}{\partial t} \qquad \text{(A1)}$$

where $k(T)$ is the thermal conductivity, $Q(T)$ is a source term, $\delta(T)$ is the density, and $C(T)$ is the specific heat. This equation is subjected to initial conditions relative to the temperature:

$$T(x, y, z) = T_0 \qquad \text{at } t = 0 \qquad \text{(A2)}$$

and relative to the convection at boundaries where it is assumed that the heat flux across the boundary surfaces is proportional to the difference between the surface temperature and the temperature T_0 of the surroundings:

$$\frac{k(T)}{\delta(T)C(T)}\frac{\partial T}{\partial n} = h[T_0 - T(x_s, y_s, z_s)] \qquad \text{(A3)}$$

where n is the outward normal to the surface, h the heat transfer coefficient at the surface and (x_s, y_s, z_s) are surface coordinates. For taking into account the water cooling at the electrodes surfaces, different values of the heat transfer coefficient h_z and h_r were used for the base surfaces and lateral surface of the disk, respectively.

The source term $Q(T)$ in eqn (A1) expresses the Joule effect and has been calculated using the equation

$$Q(T) = \frac{\varepsilon \cdot \varepsilon}{\rho(T)} \qquad \text{(A4)}$$

where ε is the electrical field and $\rho(T)$ is the resistivity. In eqn (A4), the electrical field is calculated from the two equations

$$\varepsilon = -\nabla\phi \qquad \text{(A5)}$$

and

$$\nabla^2\phi = \frac{1}{\rho(T)}(\nabla\rho \cdot \nabla\phi) \qquad \text{(A6)}$$

where ϕ is the electrical potential.

The elliptic partial differential equation of the electrical potential eqn (A6) is solved using a Gauss elimination with pivoting algorithm for banded matrices. The partial parabolic differential equation of the temperature eqn (A1) is solved using an explicit method of second-order derivatives with a stability condition bounding the time and space increments.

The stress distributions have been computed using a finite element code based on linear thermoelasticity[19] with a mesh of 400 elements.